DOI: 10.1002/ejic.201000552

Synthesis, Molecular Structure, and Physical Properties of the Complexes [{PhB(pz)$_2$(CH$_2$SMe)}$_2$M] (M = Mn^{II}, Fe^{II}; pz = pyrazol-1-yl) Containing a Novel [*N*,*N*,*S*]-Heteroscorpionate Ligand

Christian Reus,[a] Kai Ruth,[a] Sandor Tüllmann,[a] Michael Bolte,[a] Hans-Wolfram Lerner,[a] Birgit Weber,*[b] Max C. Holthausen,*[a] and Matthias Wagner*[a]

Keywords: N ligands / S ligands / Manganese / Iron / Scorpionates

Two transition metal complexes [L$_2$M] {M = Fe^{II} (**2**), Mn^{II} (**3**)} of the novel [*N*,*N*,*S*] scorpionate ligand L = [PhB(pz)$_2$(CH$_2$SMe)]$^-$ have been synthesized and characterized by X-ray crystallography, magnetic measurements, cyclic voltammetry, and various spectroscopic techniques. In the solid state, both complexes **2** and **3** possess a distorted octahedral ligand sphere, but adopt different configurations (**2**: *cis*; **3**: *trans*). According to X-ray diffraction data, Mössbauer spectroscopy, and SQUID measurements, compound **2** exists as low-spin complex in the solid state at temperatures $T \leq 20$ °C ($\mu_{eff} \approx 0.5\ \mu_B$). Upon heating, the magnetic moment μ_{eff} increases continuously to a value of 1.8 μ_B at 90 °C, which indicates a temperature dependent high-spin↔low-spin transition above room temp. Solutions of **2** in $CDCl_3$ showed paramagnetic behavior at 25 °C (μ_{eff} = 3.1 μ_B; Evans NMR method). Cyclic voltammetry (CH_2Cl_2, [Bu$_4$N][PF$_6$]; vs. FcH/FcH$^+$) on **2** reveals a reversible Fe^{II}/Fe^{III} redox transition at $E_{1/2}$ = –0.16 V. Density functional theory (B3LYP-D/def2-TZVPP//B3LYP-D/SVP level) has been used to evaluate relative energies of the *cis* and *trans* isomers of **2** in their high-spin and low-spin states. Theoretical and experimental investigations have been extended to the related literature-known homoleptic Fe^{II} complexes [{PhB(pz)$_3$}$_2$Fe], [{PhB(pz)(CH$_2$SMe)$_2$}$_2$Fe], and [{PhB(CH$_2$SMe)$_3$}$_2$Fe]. The following order of ligand-field strengths has been established: [PhB(CH$_2$SMe)$_3$]$^-$ < [PhB(pz)(CH$_2$SMe)$_2$]$^-$ < [PhB(pz)$_2$(CH$_2$SMe)]$^-$ < [PhB(pz)$_3$]$^-$. The only significant deviation from this systematic behavior became evident for the unexpectedly low solution magnetic moment of [{PhB(CH$_2$SMe)$_3$}$_2$Fe], which finds no parallel in the solid state. Computed spin-state splittings for the entire series of complexes, however, confirm the trend in solution magnetic moments and we relate the disaccording experimental observations to the presence of a second stereoisomer in crystals of [{PhB(CH$_2$SMe)$_3$}$_2$Fe] which increases the paramagnetism of solid-state samples of this complex.

Introduction

Tris(pyrazol-1-yl)borate ligands {"scorpionates"; [RB(pz)$_3$]$^-$} have found widespread use in organometallic and coordination chemistry with applications ranging from modeling active sites of metallo-enzymes through catalysis to materials sciences.[1,2] Owing to the modular synthesis approach, extensive modifications can easily be made to the ligand framework in order to optimize it for a given purpose. For example, the introduction of appropriate substituents into the 3-positions of the pyrazolyl rings allows extensive control over the steric demand of the ligand and thus over its ability to kinetically stabilize reactive complex fragments. By contrast, an adjustment of the ligand field strengths of tris(pyrazol-1-yl)borates is much harder to achieve, because electronic substituent effects on the donor properties of the pyrazolyl rings turned out to be rather modest. A more efficient way to alter the donor/acceptor properties of scorpionate ligands is to replace some or even all of their pyrazolyl rings by other donor groups.

In the context of our research, hybrid ligands [RB(pz)$_x$(CH$_2$SR′)$_{3-x}$]$^-$ containing pyrazolyl donors together with (organylthio)methyl groups are particularly important. The chemistry of these ligands was pioneered by Riordan, who described the synthesis and coordination behavior of derivatives with x = 0 and 1.[3–12] In subsequent studies, the Riordan group used selected examples of the new ligand class to prepare synthetic models for the zinc sites in methionine synthases.[10]

One focus of our own interests is the development of artificial analogs of the copper-containing enzymes dopamine β-monooxygenase (DβM) and peptidylglycine α-hydroxylating monooxygenase (PHM) as well as the detailed mechanistic understanding of the reactivity patterns of such species.[13–16] The O_2 binding mechanism of the active sites

[a] Institut für Anorganische Chemie, J. W. Goethe-Universität Frankfurt,
Max-von-Laue-Strasse 7, 60438 Frankfurt (Main), Germany
Fax: +49-69-798-29260
E-mail: Matthias.Wagner@chemie.uni-frankfurt.de
Max.Holthausen@chemie.uni-frankfurt.de
[b] Anorganische Chemie II, Universität Bayreuth,
Universitätsstrasse 30, NW I, 95440 Bayreuth, Germany
E-mail: weber@uni-bayreuth.de
Supporting information for this article is available on the WWW under http://dx.doi.org/10.1002/ejic.201000552.

of mononuclear copper enzymes was successfully modeled by use of the strongly deactivating, tripodal tetradentate N-donor ligands derived from superbasic peralkyl guanidines.[17–20] However, a more realistic ligand to mimic the protein pocket of the O_2-binding copper ion in DβM and PHM (two histidine residues, one methionine side chain) would be the yet missing scorpionate $[RB(pz)_2(CH_2SR')]^-$ (x = 2; R = Ph, R′ = Me; see above).[21] Recently, we have described the coordination behavior of $[PhB(pz)_2(CH_2SMe)]^-$ and its ditopic relative $[(pz)_3B\text{-}C_6H_4\text{-}B(pz)_2(CH_2SMe)]^{2-}$ towards Cu^I and Cu^{II} ions.[21] To assess the ligand field properties of $[PhB(pz)_2(CH_2SMe)]^-$, we have now prepared the corresponding homoleptic Fe^{II} and Mn^{II} complexes (**2**, **3**; Scheme 1). Herein we provide a detailed experimental and quantum-chemical characterization of both molecules. Particular emphasis has been put on the temperature dependence of both the spin state and the UV/Vis spectrum of **2**. The main purpose of the Mn^{II} complex **3** is to provide a system for comparison containing a divalent metal ion in a stable high-spin configuration.

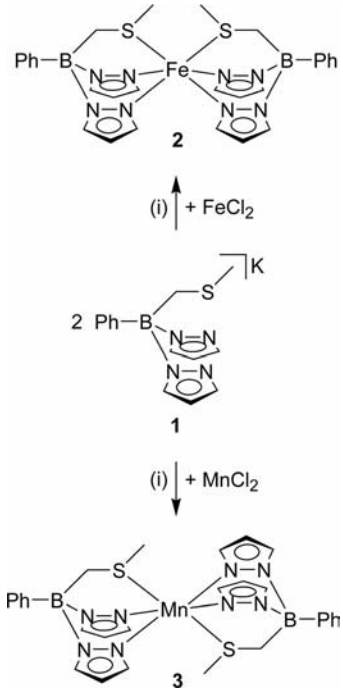

Scheme 1. Syntheses of the [*N*,*N*,*S*] scorpionate complexes **2** and **3**. (i) toluene, room temp., 6 d.

Results and Discussion

The ligand $K[PhB(pz)_2(CH_2SMe)]$ (**1**) was prepared from $PhBX_2$ (X = Cl, Br) as described previously.[21] A clean and high-yielding synthesis protocol requires the use of donor-free $Li[CH_2SMe]$,[22] because the corresponding tmeda adduct reproducibly led to considerable amounts of boronium cations $[PhB(X)(\eta^2\text{-tmeda})]^+$ as unwanted byproducts {for an X-ray crystal structure analysis of $[PhB(Cl)(\eta^2\text{-tmeda})][PhB(CH_2SMe)_3]$, cf. Figure S1 in the Supporting Information}.

Syntheses and Crystal Structure Determinations of 2 and 3

Both compounds **2** and **3** are readily available from the scorpionate ligand **1** and $FeCl_2$ or $MnCl_2$ in toluene at room temp. (Scheme 1). Irrespective of the stoichiometric ratio applied (i.e. 1:1 or 2:1), we always obtained complexes containing two ligand molecules per transition metal ion.

Single crystals were grown from pentane/toluene (**2**) and hexane/benzene (**3**). Crystal data and details of the structure determinations are summarized in Table 1.

Table 1. Crystal data and structure refinement details for **2** and **3**.

	2	**3**
Formula	$C_{28}H_{32}B_2FeN_8S_2$	$C_{28}H_{32}B_2MnN_8S_2$
fw	622.21	621.30
Color, shape	violet, block	colorless, block
Temperature /°C	–100(2)	–100(2)
Radiation	Mo-K_a, 0.71073 Å	Mo-K_a, 0.71073 Å
Crystal system	monoclinic	triclinic
Space group	*C*2/*c*	$P\bar{1}$
a /Å	12.213(2)	8.1117(10)
b /Å	12.035(2)	9.9384(11)
c /Å	20.466(4)	10.4617(12)
α /°	90	118.021(8)
β /°	100.44(3)	91.820(10)
γ /°	90	95.970(10)
V /Å^3	2958.4(10)	737.36(15)
Z	4	1
$D_{calcd.}$ /g cm^{-3}	1.397	1.399
F(000)	1296	323
μ /mm^{-1}	0.685	0.623
Crystal size /mm	0.21 × 0.18 × 0.17	0.12 × 0.11 × 0.09
Reflections collected	14526	8463
Indep. reflections (R_{int})	2782 (0.0698)	2744 (0.0655)
Data / restraints / parameters	2782 / 0 / 187	2744 / 0 / 188
GOOF on F^2	1.044	1.024
*R*1, *wR*2 [$I > 2\sigma(I)$]	0.0440, 0.0983	0.0388, 0.0905
*R*1, *wR*2 (all data)	0.0630, 0.1044	0.0534, 0.0950
Largest diff. peak and hole /e Å^{-3}	0.449/–0.361	0.696/–0.313

In the Fe^{II} complex **2**, two borate ions act as tripodal tridentate ligands (Figure 1). Thus, the molecule adopts a C_2-symmetric pseudo-octahedral structure with two sulfur and four nitrogen donors (bond angles about iron deviate by less than 4° from the ideal values of 90° and 180°).

An initially unexpected feature of the structure is its *cis* configuration. We note, however, that the exclusive formation of $[ML_2]^{cis}$ has also been reported for complexes of Fe^{II}, Co^{II}, and Ni^{II} with the related [*N*,*S*,*S*]-ligand $[PhB(pz)(CH_2SMe)_2]^-$.[9] The solid-state structure of **2** was determined at T = –100 °C and 20 °C in order to see whether the metric parameters give any indication of a spin state change in this temperature interval (a low-spin→high-spin transition should lead to an increase in the Fe–N bond lengths by about 0.15 Å[23]). We observed Fe(1)–S(1) bond lengths of 2.312(1) Å (–100 °C)/2.315(2) Å (20 °C) and

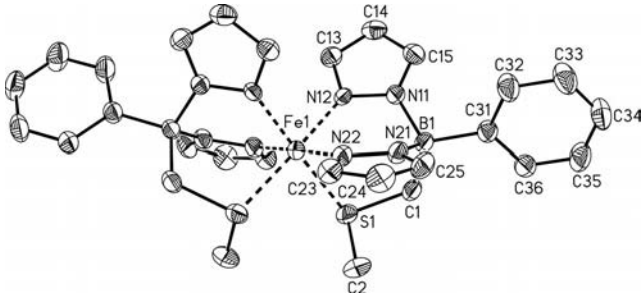

Figure 1. Molecular structure of **2** in the solid state; displacement ellipsoids at the 50% probability level. The H atoms have been omitted for clarity. Selected bond lengths [Å], bond angles [°], and torsion angles [°]: Fe(1)–N(12) 1.993(2), Fe(1)–N(22) 1.983(2), Fe(1)–S(1) 2.312(1); N(12)–Fe(1)–N(12$^{\#}$) 88.0(1), N(12)–Fe(1)–N(22) 89.7(1), N(12)–Fe(1)–N(22$^{\#}$) 91.6(1), N(12)–Fe(1)–S(1) 91.1(1), N(12)–Fe(1)–S(1$^{\#}$) 177.7(1), N(22)–Fe(1)–N(22$^{\#}$) 178.1(1), N(22)–Fe(1)–S(1) 86.3(1), N(22)–Fe(1)–S(1$^{\#}$) 92.4(1), S(1)–Fe(1)–S(1$^{\#}$) 90.0(1), B(1)···Fe(1)···B(1$^{\#}$) 167.3; B(1)–N(11)–N(12)–Fe(1) 13.2(3), B(1)–N(21)–N(22)–Fe(1) 1.5(3), B(1)–C(1)–S(1)–Fe(1) 19.7(2). Symmetry transformation used to generate equivalent atoms: #: $-x + 1$, y, $-z + 3/2$.

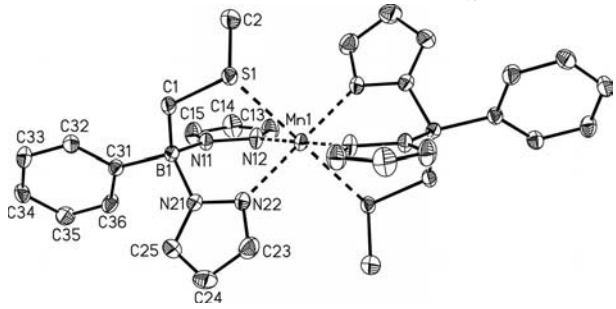

Figure 2. Molecular structure of **3** in the solid state; displacement ellipsoids at the 50% probability level. The H atoms have been omitted for clarity. Selected bond lengths [Å], bond angles [°], and torsion angles [°]: Mn(1)–N(12) 2.212(2), Mn(1)–N(22) 2.240(2), Mn(1)–S(1) 2.680(1); N(12)–Mn(1)–N(22) 85.3(1), N(12)–Mn(1)–N(22$^{\#}$) 94.7(1), N(12)–Mn(1)–S(1) 85.1(1), N(12)–Mn(1)–S(1$^{\#}$) 94.9(1), N(22)–Mn(1)–S(1) 81.7(1), N(22)–Mn(1)–S(1$^{\#}$) 98.4(1); B(1)–N(11)–N(12)–Mn(1) –6.1(3), B(1)–N(21)–N(22)–Mn(1) –23.7(3), B(1)–C(1)–S(1)–Mn(1) –9.4(2). Symmetry transformation used to generate equivalent atoms: #: $-x + 1$, $-y + 1$, $-z$.

average Fe–N bond lengths of 1.988(2) Å (–100 °C)/ 1.990(2) Å (20 °C). These values compare well with the average Fe–S distance in the all-thioether complex [{PhB($CH_2SMe)_3$}$_2$Fe] {2.303(5) Å;[5] T = –47 °C} on one hand and with the mean Fe–N bond length in [{PhB-(pz)$_3$}$_2$Fe] on the other {1.973(8) Å;[24] T = 20 °C}. In the case of [{PhB($CH_2SMe)_3$}$_2$Fe], an effective magnetic moment μ_{eff} = 1.5 μ_B was measured for a powdered sample at 20 °C,[5] whereas the tris(pyrazol-1-yl)borate complex [{PhB(pz)$_3$}$_2$Fe] is fully diamagnetic at room temp.[24] Given this background, the crystal structure of **2** points toward a low-spin state of the molecule in the crystal lattice at temperatures of 20 °C and below.

Like the Fe^{II} complex **2**, the Mn^{II} complex **3** contains two ligand molecules establishing a pseudo-octahedral coordination sphere. In contrast to **2**, **3** exists in a centrosymmetric *trans* configuration (Figure 2).

The Mn(1)–S(1) bond [2.680(1) Å] is longer by 0.368 Å than the Fe(1)–S(1) bond of **2**, and a similar effect is observed for the metal-nitrogen bonds [**3**: 2.212(2) Å/ 2.240(2) Å; **2**: 1.993(2) Å/1.983(2) Å]. The pronounced bond length elongations in **3** as compared to **2** are consistent with a d^5 high-spin state of the metal center, as confirmed by SQUID measurements; cf. also [{HB(pz)$_3$}$_2$Mn]: mean Mn–N 2.251(5) Å[25].

In both complexes, **2** and **3**, the sulfur atoms are pyramidalized with sums of bond angles of 311.2(1)° (**2**) and 314.0(1)° (**3**).

Mössbauer-, NMR- and UV/Vis Spectroscopy

Mössbauer spectra of **2** were taken at T = –193 °C and 22 °C (cf. Figure S2 in the Supporting Information). At both temperatures, the compound gives rise to a symmetric doublet with an isomer shift of δ = 0.49 mm s^{-1} (–193 °C)/ 0.42 mm s^{-1} (22 °C) and a quadrupole splitting of ΔE_Q = 0.56 mm s^{-1} (–193 °C)/0.55 mm s^{-1} (22 °C). Mössbauer spectra of a series of related tris(pyrazol-1-yl)borate complexes [{*p*-$RC_2C_6H_4B(pz^{Me})_3$}$_2$Fe] have been published by Reger et al. (pz^{Me}: 3-methylpyrazol-1-yl).[26] The derivative with R = Ph undergoes a thermally induced spin state crossover and contains a low-spin Fe^{II} ion at –195 °C (δ = 0.54 mm s^{-1}, ΔE_Q = 0.41 mm s^{-1}) but high-spin Fe^{II} at 22 °C (δ = 1.00 mm s^{-1}, ΔE_Q = 3.66 mm s^{-1}). In the light of these results and in agreement with the conclusions drawn from the X-ray crystal structure analysis of **2**, the Mössbauer parameters of solid **2** are clearly indicative of Fe^{II} ions in the low-spin state (for $T \leq$ 22 °C).

At room temp., the ^{1}H NMR spectrum of **2** in [D_8]toluene is characterized by broad signals with chemical shifts between 0 and 35 ppm. This observation suggests that under these conditions, **2** is not entirely in its diamagnetic low-spin state, but that a paramagnetic high-spin state is energetically accessible and populated to some extent. Accordingly, the signal range decreases continuously upon cooling, until, at a temperature of –70 °C, reasonably well-resolved proton resonances were obtained in a spectral region characteristic of diamagnetic poly(pyrazol-1-yl)borate complexes. The most important features of the low-temperature spectrum are the following: (1) the integral ratio between the pyrazolyl and the (methylthio)methyl protons is in agreement with the proposed 2:1 stoichiometry. (2) The methylene protons B-CH_2-S appear as two doublets (δ =1.79 ppm, 1.57 ppm; $^2J_{HH}$ = 13.5 Hz) which indicates that the Fe–S bonds are retained in solution. (3) Two signal sets (ratio 1:1) are observed for the pyrazolyl rings, but only one set of signals appears for the (methylthio)methyl groups. This feature is consistent both with a *cis* and with a *trans* configuration of the complex. However, it rules out that mixtures of isomers are present in solution. The ^{13}C NMR spectroscopic data are in full accord with the conclusions drawn from the proton NMR spectra.

Complex **2** possesses a blue color at room temp. in solution and in the solid state. Corresponding bands in the visible region of the electronic spectrum appear at λ_{max} = 573 nm and 404 nm with small extinction coefficients of ε = 35 and 59 $M^{-1}cm^{-1}$, respectively. Upon heating, the intensity of both bands continuously decreases [T = 70 °C: ε(573) = 14 and ε(404) = 24 $M^{-1}cm^{-1}$; Figure 3].

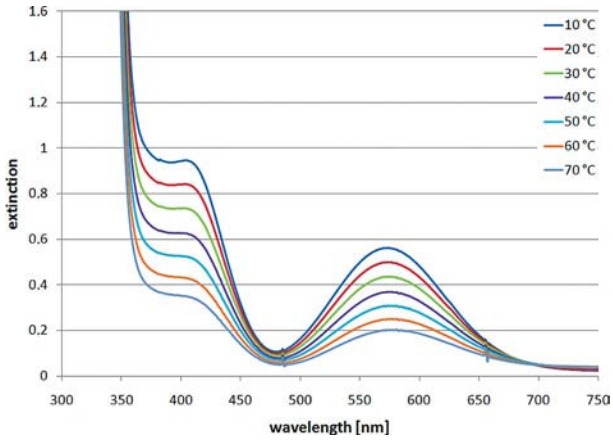

Figure 3. Variable-temperature electronic spectrum of **2** in toluene (c = 14.38 mmol L^{-1}).

A similar temperature dependence is also known for complexes [$Fe^{II}L_2$] containing two tris(pyrazol-1-yl)borate ligands L and has been attributed to the transition between the low-spin $^1A_{1g}$ ($t_{2g}^6e_g^{*0}$) state and the typically colorless or lightly colored high-spin $^5T_{2g}$ ($t_{2g}^4e_g^{*2}$) state.[27] Given this background and the small extinction coefficients, the two visible absorptions are assigned to the Laporte-forbidden, spin-allowed d-d transitions $^1A_{1g}\rightarrow{}^1T_{1g}$ (573 nm) and $^1A_{1g}\rightarrow{}^1T_{2g}$ (404 nm) in pseudo-octahedral **2** (Table 2). The all-sulfur complex [{PhB($CH_2SMe)_3$}$_2$Fe][5] exhibits the corresponding two absorptions at λ_{max} = 627 nm (33 $M^{-1}cm^{-1}$; $^1A_{1g}\rightarrow{}^1T_{1g}$) and 439 nm (56 $M^{-1}cm^{-1}$; $^1A_{1g}\rightarrow{}^1T_{2g}$), the [*N*,*S*,*S*] complex [{PhB(pz)($CH_2SMe)_2$}$_2$-Fe][28] at 597 nm (23 $M^{-1}cm^{-1}$) and 421 nm (39 $M^{-1}cm^{-1}$). The all-nitrogen complex [{PhB($pz)_3$}$_2$Fe][29] shows its $^1A_{1g}\rightarrow{}^1T_{1g}$ transition at λ_{max} = 530 nm (100 $M^{-1}cm^{-1}$; re-measured in toluene) while the $^1A_{1g}\rightarrow{}^1T_{2g}$ transition is hidden underneath very intense metal-to-ligand charge-transfer bands.

Table 2. Electronic spectra of [{PhB($CH_2SMe)_3$}$_2$Fe][a], [{PhB(pz)($CH_2SMe)_2$}$_2$Fe][b],[28] compound **2**[c], and [{PhB($pz)_3$}$_2$-Fe][c].

	$^1A_{1g}\rightarrow{}^1T_{1g}$ [nm]	$^1A_{1g}\rightarrow{}^1T_{2g}$ [nm]	D_q [cm^{-1}]	B [cm^{-1}]
[{PhB($CH_2SMe)_3$}$_2$Fe]	627	439	1763	420
[{PhB(pz)($CH_2SMe)_2$}$_2$Fe]	597	421	1850	438
2	573	404	1928	456
[{PhB($pz)_3$}$_2$Fe]	530	–	–	–

[a] $CHCl_3$. [b] CH_2Cl_2. [c] Toluene.

Assuming C = 4B, the crystal-field strengths D_q and the Racah parameter B were calculated using the equations (i) $^1A_{1g}\rightarrow{}^1T_{1g}$ = 10 D_q – C and (ii) $^1A_{1g}\rightarrow{}^1T_{2g}$ = 10 D_q – C + 16 B.[30,31] These data, which are compiled in Table 2, suggest the following order of ligand-field strengths: [PhB($CH_2SMe)_3$]$^-$ < [PhB(pz)($CH_2SMe)_2$]$^-$ < [PhB($pz)_2$-(CH_2SMe)]$^-$ < [PhB($pz)_3$]$^-$.

Characterization of Magnetic Properties

Magnetic susceptibilities were determined both in the solid state (SQUID measurements) and in solution (Evans NMR method[32,33]).

In the case of the Mn^{II} complex **3**, the expected d^5 high-spin state was confirmed.

Bulk crystalline samples of **2** are largely diamagnetic at temperatures $T \leq$ 20 °C ($\mu_{eff} \approx$ 0.5 μ_B; Figure 4), as has already been deduced from X-ray crystallography and Mössbauer spectroscopy.

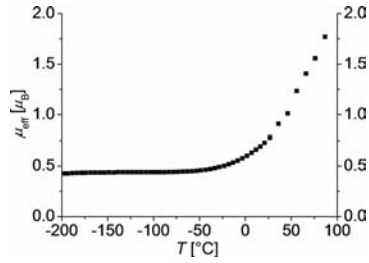

Figure 4. Plot of μ_{eff} vs. T for the Fe^{II} complex **2**.

Upon heating to approximately 90 °C, μ_{eff} increases continuously to a value of 1.8 μ_B. This is an indication for a temperature-dependent high-spin↔low-spin transition above room temp. in the solid state. To estimate $T_{1/2}$, the data were analyzed assuming a gradual spin transition. The fit of γ_{HS} vs. T is presented in the Supporting Information (Figure S3) together with the parameters used. These data suggest that $T_{1/2}$ is in the region of 180 °C. In the crystal lattice, the related [*S*,*S*,*S*] complex [{PhB($CH_2SMe)_3$}$_2$Fe] tends to be more paramagnetic than **2** [μ_{eff} = 1.3 μ_B (–73 °C), 1.5 μ_B (25 °C), 2.3 μ_B (90 °C), 3.2 μ_B (127 °C); Figure 5].[5]

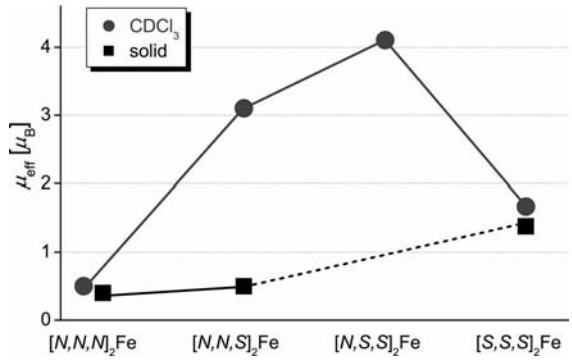

Figure 5. Magnetic moments of the complexes [{PhB($pz)_x$-($CH_2SMe)_{3-x}$}$_2$Fe] (x = 0–3). Circles: values obtained in $CDCl_3$ solution at 25 °C using the Evans NMR method; squares: values determined in the solid state by SQUID measurements (25 °C).

In $CDCl_3$ solution, **2** possesses a magnetic moment μ_{eff} of 3.1 μ_B at 25 °C, which equals a number of unpaired electrons N' of approximately N' = 1.8. Pure high-spin (N' =

4) and low-spin ($N' = 0$) Fe^{II} states are associated with magnetic moments of about 5.2 μ_B and 0.4 μ_B, respectively (experimentally determined values).[26] The magnetic moment of **2** is higher than that of the tris(pyrazol-1-yl)borate complex [{PhB(pz)$_3$}$_2$Fe], which has been reported to be fully diamagnetic in $CDCl_3$ at room temp.[29] On the other hand, the population of the high-spin state in the [*N*,*N*,*S*] species **2** is lower than in the case of the [*N*,*S*,*S*] complex [{PhB(pz)(CH$_2$SMe)$_2$}$_2$Fe] (μ_{eff} = 4.1 μ_B; $CDCl_3$).[28] In view of the trend in the ligand-field strengths along the series of [N_xS_{3-x}] scorpionates, one should expect a further increase in μ_{eff} in the [*S*,*S*,*S*] complex [{PhB(CH$_2$SMe)$_3$}$_2$Fe]. Surprisingly, however, a small magnetic moment of only 1.6 μ_B at 27 °C in $CDCl_3$ was reported for this compound[5] (Figure 5; we have resynthesized [{PhB(CH$_2$SMe)$_3$}$_2$Fe] to redetermine the magnetic moment and fully reproduced the published value).

Electrochemical Measurements

Cyclic voltammograms of **2** and the reference compound [{PhB(pz)$_3$}$_2$Fe] were measured with two different supporting electrolytes, i.e. [Bu_4N][PF_6] and [Bu_4N][B(C_6F_5)$_4$]. Data obtained with the [PF_6] salt are useful for comparison with literature values of related complexes; redox potentials recorded on solutions containing the [B(C_6F_5)$_4$] salt are helpful for an assessment of counterion effects on key electrochemical parameters. The Fe^{II}/Fe^{III} redox transitions of **2** and [{PhB(pz)$_3$}$_2$Fe] are electrochemically reversible on the cyclic voltammetric timescale as evidenced by the following criteria: the current ratios i_{pc}/i_{pa} are constantly equal to 1, the current functions $i_{pa}/v^{1/2}$ remain constant, and the peak-to-peak separations ΔE are similar to the value found for the internal ferrocene standard. Along the sequence [{PhB(CH$_2$SMe)$_3$}$_2$Fe]→**2**→[{PhB(pz)$_3$}$_2$Fe] we find a continuous cathodic shift of the Fe redox potential (Table 3), indicating that an increasing number of pyrazolyl donors leads to more electron-rich Fe^{II} ions.

Table 3. Electrochemical data of [{PhB(CH$_2$SMe)$_3$}$_2$Fe],[5] **2**, and [{PhB(pz)$_3$}$_2$Fe] in CH_2Cl_2 vs. FcH/FcH^+ measured at a scan rate of 0.10 V s^{-1}.

	$E_{1/2}$ [V][a]	ΔE [mV][a]	$E_{1/2}$ [V][b]	ΔE [mV][b]
[{PhB(CH$_2$SMe)$_3$}$_2$Fe]	0.09	96	–	–
2	–0.16	77	–0.22	72
[{PhB(pz)$_3$}$_2$Fe]	–0.29	80	–0.36	70

[a] [Bu_4N][PF_6]. [b] [Bu_4N][B(C_6F_5)$_4$].

Moreover, we note that a change of the supporting electrolyte from [Bu_4N][PF_6] to [Bu_4N][B(C_6F_5)$_4$] results in cathodic shifts of the redox potentials of **2** and [{PhB(pz)$_3$}$_2$Fe] by 0.06 V and 0.07 V, respectively. This leads to the conclusion that counterion effects must not be neglected in the redox chemistry of both complexes even though the Fe centers are well shielded from the surrounding solution by their octahedral ligand sphere.

Quantum Chemical Calculations

The experimental results reported thus far leave several questions unresolved, which we decided to tackle by quantum chemical means: (i) We optimized the structures of the *cis* and *trans* isomers of **2** and **3** to assess their preferred constitution in solution. (ii) To evaluate the stability of the quasi-octahedral, six-coordinate framework of **2**, we performed additional calculations on five-coordinate isomers, which are obtained by decoordinating individual ligand arms. (iii) The solid-state magnetic moments along the series [{PhB(pz)$_3$}$_2$Fe]→**2**→[{PhB(CH$_2$SMe)$_3$}$_2$Fe] are consistent with the expected qualitative trend in the ligand-field strengths of these scorpionates (successive exchange of the stronger *N*-donor ligands by the weaker *S*-donor ligands should lead to progressively more stable high-spin states). In contrast, the corresponding magnetic moments in solution do not show a similar monotonous increase (Figure 5). This leads to the question: Are the μ_{eff} values of **2** and [{PhB(pz)(CH$_2$SMe)$_2$}$_2$Fe] irregularly high, or is the magnetic moment of [{PhB(CH$_2$SMe)$_3$}$_2$Fe] irregularly low? To address the puzzling results of the magnetic measurements in some detail we performed calculations on high-spin (quintet) and low-spin (singlet) states of all conceivable isomers of the compounds [{PhB(pz)$_x$(CH$_2$SMe)$_{3-x}$}$_2$Fe] (x = 0–3). In this way we were able to obtain information on the intrinsic magnetic properties of this series of compounds, free of potentially complicating effects of solvent or counterion molecules.

The current literature witnesses that an accurate quantum chemical assessment of absolute values for spin-state energy differences remains a formidable task as of today. A number of recent studies was concerned with the identification of an optimal density functional approach for the proper assessment of spin-crossover Fe^{II} complexes.[34–40] Although a few promising functionals surface in these studies, a clear recommendation is hard to recognize. For the present set of systems we tested several functional/basis set combinations but, as detailed in the Supporting Information, none gave fully satisfying results. However, to rationalize the magnetic behavior of the species under study it suffices here to focus our discussion on the *relative* changes in computed spin-state splittings that occur upon variation of the ligand environment. To this end, the choice of method is far less critical since many functionals yield systematic errors that cancel out to a large extent if trends in spin-state splittings for a series of related complexes are considered.[39,40] Results discussed in the following are based on single point energy calculations at the B3LYP-D/def2-TZVPP level of density functional theory. These calculations were performed on structures optimized at the B3LYP-D/SVP level, which gave excellent agreement with experimental structures (see Supporting Information). Owing to the inherent tendency of the B3LYP functional to artificially favor the stability of high-spin over low-spin states,[34–38] computed *absolute* energy differences reported below for the individual complexes are probably shifted somewhat into the high-spin region. To assess the influence

of dielectric solvation effects we applied the COSMO continuum solvent model (solvent CH_2Cl_2), but in all cases this left isomer stabilities and spin state splittings essentially unaffected (cf. Table 4). For the sake of conciseness the discussion of results is based on computed gas phase data only.

Table 4. Compilation of computed results on the Fe^{II} scorpionate complexes under investigation here (the Mn^{II} complex **3** has been included for comparison); energies (in kcal mol^{-1}) are given relative to the most stable isomer in its electronic ground state.

	E_{rel} (ls/hs)	$E_{rel,COSMO}$ (ls/hs)
[N_6]	0.0/4.3	0.0/4.5
[N_4S_2]^{cis} (2^{cis})	0.6/0.0	0.0/0.1
[N_4S_2]^{trans} (2^{trans})	4.1/3.7	4.0/2.7
[N_2S_4]^{cis}	10.2/3.1	9.8/2.7
[N_2S_4]^{trans}	8.9/0.0	9.3/0.0
[S_6]^{meso}	5.4/0.0	5.7/0.0
[S_6]^{rac}	10.7/2.3	11.2/2.5
3^{cis}	21.8/0.0	–
3^{trans}	24.7/2.5	–

Relative Energies of cis and trans Isomers of 2 and 3

We optimized the structures of the respective *cis* and *trans* isomers of **2** and **3** in both, low-spin and high-spin states (Table 4). In line with the crystallographic findings our calculations corroborate that, in the low-spin (ls) state, **2^{cis}** is lower in energy than **2^{trans}** by $\Delta E^{trans-cis}$ = 3.5 kcal mol^{-1}. All bond lengths in the optimized structure of **2^{cis}**(ls) agree well with the results of the single-crystal X-ray structure analysis (Figure 6).

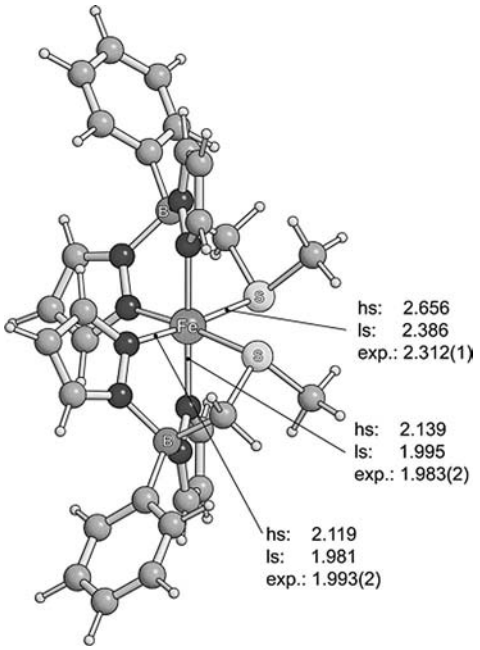

Figure 6. Selected bond lengths in the optimized ls and hs structures of **2^{cis}** (B3LYP-D/SVP level).

A comparable energy difference of $\Delta E^{trans-cis}$ = 3.7 kcal mol^{-1} results for the two isomers of **2** in the high-spin (hs) state. The optimized structure of **2^{cis}**(hs) exhibits the expected elongation of metal-ligand bond lengths (Figure 6), and the average increase of the Fe–N bond lengths of 0.14 Å is perfectly in line with expectation.[23] The calculations reveal only small energy differences between the high-spin and low-spin states (ΔE_{hs-ls}) of both isomers (**2^{cis}**: ΔE_{hs-ls} = –0.6 kcal mol^{-1}; **2^{trans}**: ΔE_{hs-ls} = –0.4 kcal mol^{-1}). For the corresponding Mn^{II} complex **3** substantially larger spin state splittings result from the calculations and both isomers clearly exhibit a high-spin ground state (**3^{cis}**: ΔE_{hs-ls} = –21.8 kcal mol^{-1}; **3^{trans}**: ΔE_{hs-ls} = –22.2 kcal mol^{-1}). As for the iron complex **2** we find the **3^{cis}**(hs) isomer slightly more stable than **3^{trans}**(hs). The minute energy difference of $\Delta E^{trans-cis}$ = 2.5 kcal mol^{-1} is, however, sufficiently small to conclude that the solid-state structure of **3**, which exhibits a *trans*-configuration, is dominated by crystal packing forces.

Structural Integrity of 2 in Solution

The energies required to decoordinate one *N*- or *S*-donor arm have been calculated for both isomers of **2** in their respective low-spin and high-spin states. For the low-spin isomers all reorganization energies (c.n. 6 → c.n. 5) are prohibitively high (ΔE > 12 kcal mol^{-1}). For the corresponding high-spin structures, all geometry optimizations on *N*-decoordinated isomers lead back to six-coordinate structures. The energetically lowest lying five-coordinate high-spin isomer with one decoordinated *S*-donor arm is 5.0 kcal mol^{-1} less stable than **2^{cis}** in its computed high-spin ground state (the structure of this five-coordinate [N_4S_1] high-spin complex is shown in the Supporting Information). These results do not indicate that any significant population of **2** gives up its constitution as intact six-coordinate Fe^{II} complexes in quasi-octahedral coordination geometries, which supports the assumptions made to interpret the solution UV/Vis spectra of complex **2**.

Magnetic Properties of [{PhB(pz)$_3$}$_2$Fe], 2, [{PhB(pz)-(CH$_2$SMe)$_2$}$_2$Fe], and [{PhB(CH$_2$SMe)$_3$}$_2$Fe] in Solution

To gain further insight into the magnetic properties of the complexes [{PhB(pz)$_x$(CH$_2$SMe)$_{3-x}$}$_2$Fe] (x = 0–3), we performed calculations on the entire homologous series, i.e., [{PhB(pz)$_3$}$_2$Fe] (**[N_6]**), [{PhB(pz)$_2$(CH$_2$SMe)}$_2$Fe] (**2** = **[N_4S_2]**), [{PhB(pz)(CH$_2$SMe)$_2$}$_2$Fe] (**[N_2S_4]**), and [{PhB-(CH$_2$SMe)$_3$}$_2$Fe] (**[S_6]**). Table 4 shows the computed relative spin state energies.

In agreement with experimental results put forward by Jesson et al.,[29] we obtained a diamagnetic low-spin ground state for the **[N_6]** complex; the corresponding high-spin paramagnetic state lies 4.3 kcal mol^{-1} higher in energy. As already discussed above, almost degenerate spin states resulted for the *cis* and the *trans* isomers of **[N_4S_2]**, with slightly more stable high-spin states {by 0.6 kcal mol^{-1} (**[N_4S_2]^{cis}**) and 0.4 kcal mol^{-1} (**[N_4S_2]^{trans}**)}. For both isomers of **[N_2S_4]**, we computed high-spin ground states, which are separated from the low-spin states by 7.1 kcal mol^{-1} (**[N_2S_4]^{cis}**) and 8.9 kcal mol^{-1} (**[N_2S_4]^{trans}**). Inspection of the crystal structure of **[S_6]**[5] brought to light a disorder of all six sulfur atoms over two positions with equal occupancy

factors. The corresponding cobalt complex[5] does not suffer from similar disorder but shows a well-defined canting of all six SMe groups in the same rotational direction (*meso* conformation, cf. Figure 7). We therefore applied this conformation for initial calculations on the iron complex $[S_6]^{meso}$. We assign a high-spin ground state to $[S_6]^{meso}$ but we find a *smaller* energy difference to the low-spin state (5.4 kcal mol^{-1}) than for the $[N_2S_4]$ isomers.

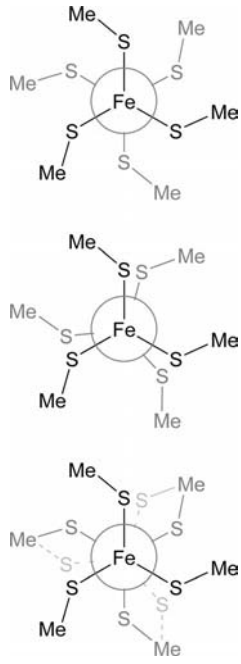

Figure 7. Schematic illustration of the ligand arrangements in $[S_6]^{meso}$ (top) and $[S_6]^{rac}$ (middle), and a superposition of both structures (bottom), which mimics the disorder observed in the X-ray crystal structure of [{PhB(CH$_2$SMe)$_3$}$_2$Fe].

Up to this point our theoretical findings reproduce the trend in solution magnetic moments along the series $[N_6]$ to $[S_6]$, but clearly not the markedly different monotonous increase of the magnetic moments in the solid state. Given the suspiciously close experimental values obtained for $[S_6]$ in solution and in the solid state, we conjectured that the severe disorder present in the crystal lattice could have a non-negligible influence on the solid-state magnetic moment. While we initially assumed that the reason for the disorder was a mere superposition of two *meso* molecules, we found that the presence of a *rac* stereoisomer (cf. Figure 7) would also be in accordance with the X-ray crystal structure data. Calculations on the corresponding complex $[S_6]^{rac}$ give a high-spin ground state as in $[S_6]^{meso}$, but at the same time indicate a significantly larger energy gap to the low-spin configuration (8.4 kcal mol^{-1}). Comparing the relative energies of the respective high-spin structures we find that $[S_6]^{rac}$ is less stable than $[S_6]^{meso}$ by 2.3 kcal mol^{-1}.

Based on these results we suggest the following explanation for the qualitatively different trends observed for the magnetic moments of $[N_6]$ to $[S_6]$ in solution and in the solid state: Assuming a pronounced conformational flexibility of the SMe groups, solutions of the complex [{PhB(CH$_2$SMe)$_3$}$_2$Fe] should be dominated by the $[S_6]^{meso}$ conformer, which is thermodynamically favored over the $[S_6]^{rac}$ stereoisomer. While an energy difference of 2.3 kcal mol^{-1} suffices to explain the lack of significant populations of $[S_6]^{rac}$ in solution, this rather small energy difference might well be overcome in the solid state where crystal packing forces come into play. The assumption that a non-negligible fraction of the complex [{PhB(CH$_2$SMe)$_3$}$_2$Fe] exists as $[S_6]^{rac}$ in the crystal lattice provides a straightforward rationale for the observation of an increased paramagnetism for this species in the solid state.

We thus suggest that the trends in magnetic moments measured in solution reflect the intrinsic magnetic properties of the thermodynamically most stable (stereo)isomers of the complexes under study. We further suggest that deviations from the intuitively expected trend (i.e., a successive decrease of ligand donor strengths from $[N_6]$ to $[S_6]$ should lead to parallel development of magnetic moments as observed in the solid state) are most likely a consequence of steric interactions present in the complexes $[N_2S_4]$ and $[N_4S_2]$, which destabilize the more compact low-spin structures with respect to the more expanded high-spin structures. In both species, repulsive interactions cannot be relieved as efficiently as in the $[S_6]$ isomers by optimal alignment of the ligand environment due to the presence of the conformationally rigid pyrazolyl groups. We note in passing that for the isomers of $[N_2S_4]$ and $[N_4S_2]$ we did not find any alternative low energy structures with different orientations of the SMe groups.

Conclusions

With the synthesis of the [*N*,*N*,*S*] scorpionate [PhB(pz)$_2$(CH$_2$SMe)]$^-$, the homologous series of smoothly varying ligands [PhB(pz)$_x$(CH$_2$SMe)$_{3-x}$]$^-$ (x = 0–3) has been completed. Using the octahedral Fe^{II} complex [{PhB(pz)$_2$(CH$_2$SMe)}$_2$Fe] as a representative example, we have shown by X-ray crystallography, magnetic measurements, cyclic voltammetry, and various spectroscopic techniques that a gradual fine-tuning of key physical parameters (e.g. redox potentials, spin state, UV/Vis absorptions) is possible by choice of the ligand with the best-suited donor set. The following order of ligand-field strengths has been established: [PhB(CH$_2$SMe)$_3$]$^-$ < [PhB(pz)(CH$_2$SMe)$_2$]$^-$ < [PhB(pz)$_2$(CH$_2$SMe)]$^-$ < [PhB(pz)$_3$]$^-$.

DFT calculations on [{PhB(pz)$_x$(CH$_2$SMe)$_{3-x}$}$_2$Fe] (x = 0–3) at the B3LYP-D/def2-TZVPP//B3LYP-D/SVP level are in pleasingly good agreement with experimental findings on molecular structures and trends in solution magnetic moments. The fact that the qualitative trend in solution magnetic moments is not paralleled by the solid-state magnetic moments can be resolved by the assumption that in solution $[S_6]$ adopts the thermodynamically favored *meso* conformation, whereas in the crystal lattice a significant proportion

of the molecules adopt the *rac* conformation. This results in increased paramagnetism of the sample because, according to the quantum chemical analysis, the low-spin state is significantly more disfavored for $[S_6]^{rac}$ compared to $[S_6]^{meso}$.

Experimental Section

General Considerations: All reactions and manipulations of air-sensitive compounds were carried out in dry, oxygen-free nitrogen or argon using standard Schlenk ware. Solvents were freshly distilled under argon from Na-benzophenone (toluene) or Na/Pb alloy (pentane, hexane). UV/Vis: Varian Cary 50 Scan UV/Vis Spectrophotometer; Mössbauer: own construction, TU München; Magnetic Measurements: Quantum-Design-MPMSR-XL-SQUID-Magnetometer; NMR: Bruker AMX 400, Bruker AMX 250, Bruker DPX 250 spectrometers. $^{11}B\{^1H\}$ NMR spectra are reported relative to external $BF_3{\cdot}Et_2O$. Abbreviations: d = doublet, m = multiplet, br. = broad. Compound **1** was synthesized according to a literature procedure.[21]

Synthesis of 2: Compound **1** (0.071 g, 0.22 mmol) and $FeCl_2$ (0.015 g, 0.12 mmol) were suspended in toluene (25 mL). The reaction mixture was stirred for 6 d at room temp. After centrifugation, the blue-grey supernatant was evaporated to dryness in vacuo to give a dark purple microcrystalline solid. Dark blue single crystals were obtained by slow diffusion of pentane into a toluene solution of **2**. Yield: 0.050 g (73%). ^1H NMR ([D$_8$]toluene, 250.1 MHz, –70 °C): δ = 7.80 (m, 4 H, PhH), 7.64 (br., 2 H, pzH-3 or 5), 7.57–7.41 (m, 8 H, PhH, pzH-3 or 5), 7.36, 6.75 (2 × br., 2 × 2 H, pzH-3′,5′), 6.05 (br., 2 H, pzH-4), 5.92 (br., 2 H, pzH-4′), 1.79, 1.57 (2 × d, $^2J_{HH}$ = 13.5 Hz, 2 × 2 H, BCH_2), 0.79 (br., 6 H, SCH_3) ppm. $^{13}C\{^1H\}$ NMR ([D$_8$]toluene, 62.9 MHz, –70 °C): δ = 149.0 (pzC-3 or 5), 147.4 (pzC-3′ or 5′), 145.2 (PhC-*i*), 139.1 (pzC-3 or 5), 137.8 (pzC-3′ or 5′), 134.7, 128.0, 128.0 (PhC), 106.8 (pzC-4′), 106.4 (pzC-4), 24.3 (br., BCH_2), 21.4 (SCH_3) ppm. $^{11}B\{^1H\}$ NMR ([D$_8$]toluene, 80.3 MHz, –70 °C): δ = –0.2 ($h_{1/2}$ = 1900 Hz) ppm. UV/Vis (toluene; 293 °C): λ_{max} (ε) = 573 (35), 404 nm (59 $M^{-1}cm^{-1}$). $C_{28}H_{32}B_2FeN_8S_2$ [622.21]: calcd. C 54.05, H 5.18, N 18.01; found C 54.10, H 5.32, N 17.98.

Synthesis of 3: Compound **1** (0.100 g, 0.31 mmol) and $MnCl_2$ (0.020 g, 0.16 mmol) were suspended in toluene (15 mL). The reaction mixture was stirred for 6 d at room temp. After centrifugation, the pale yellow supernatant was evaporated to dryness in vacuo to give a colorless solid foam. Colorless single crystals were obtained by slow diffusion of hexane into a benzene solution of **3**. Yield: 0.019 g (20%). $C_{28}H_{32}B_2MnN_8S_2$ [621.30]: calcd. C 54.13, H 5.19, N 18.04; found C 54.08, H 5.37, N 18.13.

Crystal Structure Determinations of [PhB(Cl)(η^2-tmeda)][PhB(CH$_2$SMe)$_3$], 2, and 3: Data collections were performed on a Stoe-IPDS-II two-circle-diffractometer with graphite-monochromated Mo-K_α radiation. Empirical absorption corrections with the MULABS[41] option in the program PLATON[42] were performed. The structures were solved by direct methods[43] and refined with full-matrix least-squares on F^2 using the program SHELXL97.[44] Hydrogen atoms were placed on ideal positions and refined with fixed isotropic displacement parameters using a riding model.

CCDC-768503 (for [PhB(Cl)(η^2-tmeda)][PhB(CH$_2$SMe)$_3$]), -768501 (for **2**, T = –100 °C), -768734 (for **2**, T = 20 °C), and -768502 (for **3**) contain the supplementary crystallographic data for this paper. These data can be obtained free of charge from The Cambridge Crystallographic Data Centre via www.ccdc.cam.ac.uk/data_request/cif.

Magnetic measurements were performed on a Quantum-Design-MPMSR-XL-SQUID-Magnetometer in a temperature range from –268 °C to 87 °C. All measurements were carried out at two field strengths (0.2 T and 0.5 T) in the settle mode. The data were corrected for the magnetisation of the sample holder and diamagnetic corrections were estimated using Pascal's constants.

Mössbauer spectra have been recorded using a conventional Mössbauer spectrometer operating in the sinusoidal acceleration mode. The sample was placed in an Oxford bath cryostat.

Electrochemical Measurements: All measurements were performed with an EG&G Princeton Applied Research 263A potentiostat on carefully dried (CaH_2) and degassed CH_2Cl_2 solutions containing 0.05 M $[Bu_4N][B(C_6F_5)_4]$ or 0.10 M $[Bu_4N][PF_6]$ as supporting electrolyte. A 2 mm diameter Pt-disc working electrode was used for **2** and a 3 mm GC-disc working electrode for **3**. The experiments were performed with scan rates between 0.2 Vs^{-1} and 0.05 Vs^{-1}; reported values were recorded with a scan rate of 0.1 Vs^{-1} and referenced against internal ferrocene.

Quantum Chemical Calculations: Density functional theory calculations have been performed employing the B3LYP-D[45–48] functional, which includes empirical corrections for dispersive effects. Further calculations were done with the B3LYP* functional, which was specifically devised for an improved description of spin state energies,[49] without compromising its performance[50] for the assessment of thermochemical properties. Finally, we used the OPBE functional,[51,52] which was advertised as useful method to describe spin-state energies of closely related systems.[35] Starting structures for geometry optimizations were constructed from X-ray structures if available. Geometry optimizations and subsequent harmonic frequency calculations were performed using Gaussian09.[53] Here, the dispersion-corrected[54] B3LYP-D functional was used in combination with the SVP[55,56] basis set. Further calculations were performed with the TZVP[55,56] basis set (see Supporting Information). To obtain converged energies, single point calculations were done with the larger def2-TZVPP[57] basis set utilizing the ORCA[58] program. In these calculations the latest 2010 parametrization[59] of dispersion corrections was employed. To speed up the calculations, the RIJCOSX approximation[60–62] was used in conjunction with the def2-TZV/J[63] auxiliary basis set. Wave functions were converged using tight convergence criteria and fine integration grids (ORCA keywords "tightscf, grid4, gridx4") throughout and the spin unrestricted formalism was used for open shell situations. To assess the influence of dielectric solvation effects on our results we applied the COSMO continuum solvent model[64] (solvent CH_2Cl_2), but in all cases this left isomer stabilities and spin state splittings essentially unaffected (cf. Table 4). For the sake of conciseness the discussion of results is based on computed gas phase data only.

Supporting Information (see footnote on the first page of this article): X-ray crystal structure analysis of [PhB(Cl)(η^2-tmeda)]-[PhB(CH$_2$SMe)$_3$]; crystallographic data of **2** (determined at –100 °C and 20 °C) and **3** in CIF format; Mössbauer spectra of **2** at –193 °C and 22 °C; fit of γ_{HS} vs. T for **2** with the used parameters indicated; assessment of DFT methods; calculated structure of the five-coordinate $[N_4S_1]$ isomer of **2**; xyz-coordinates of all calculated molecular structures.

Acknowledgments

This research was generously supported by the Deutsche Forschungsgemeinschaft (DFG) (SFB/TRR 49) and the Fonds der Chemischen Industrie (FCI). K. R. wishes to thank the Degussa Stiftung for a Ph.D. grant. The authors would like to thank K. Achterhold (TU München) for the acquisition of Mössbauer spectra. We are grateful to Prof. Dr. C. G. Riordan for helpful discussions. The allotment of computer time by the CSC Frankfurt and the HHLR Darmstadt, as well as their excellent service is gratefully acknowledged.

[1] S. Trofimenko, *Chem. Rev.* **1993**, *93*, 943–980.
[2] a) S. Trofimenko, *Scorpionates - The Coordination Chemistry of Polypyrazolylborate Ligands*, Imperial College Press, London, **1999**; b) C. Pettinari, *Scorpionates II: Chelating Borate Ligands*, Imperial College Press, London, **2008**.
[3] C. G. Riordan, *Coord. Chem. Rev.* **2010**, *254*, 1815–1825.
[4] P. Ge, B. S. Haggerty, A. L. Rheingold, C. G. Riordan, *J. Am. Chem. Soc.* **1994**, *116*, 8406–8407.
[5] C. Ohrenberg, P. Ge, P. Schebler, C. G. Riordan, G. P. A. Yap, A. L. Rheingold, *Inorg. Chem.* **1996**, *35*, 749–754.
[6] C. Ohrenberg, M. M. Saleem, C. G. Riordan, G. P. A. Yap, A. K. Verma, A. L. Rheingold, *Chem. Commun.* **1996**, 1081–1082.
[7] C. Ohrenberg, C. G. Riordan, L. Liable-Sands, A. L. Rheingold, *Coord. Chem. Rev.* **1998**, *174*, 301–311.
[8] P. J. Schebler, C. G. Riordan, I. A. Guzei, A. L. Rheingold, *Inorg. Chem.* **1998**, *37*, 4754–4755.
[9] S.-J. Chiou, P. Ge, C. G. Riordan, L. M. Liable-Sands, A. L. Rheingold, *Chem. Commun.* **1999**, 159–160.
[10] S.-J. Chiou, J. Innocent, C. G. Riordan, K.-C. Lam, L. Liable-Sands, A. L. Rheingold, *Inorg. Chem.* **2000**, *39*, 4347–4353.
[11] C. Ohrenberg, L. M. Liable-Sands, A. L. Rheingold, C. G. Riordan, *Inorg. Chem.* **2001**, *40*, 4276–4283.
[12] K. Fujita, A. L. Rheingold, C. G. Riordan, *Dalton Trans.* **2003**, 2004–2008.
[13] P. Spuhler, M. C. Holthausen, *Angew. Chem.* **2003**, *115*, 6143–6147; *Angew. Chem. Int. Ed.* **2003**, *42*, 5961–5965.
[14] P. Milko, J. Roithová, D. Schröder, J. Lemaire, H. Schwarz, M. C. Holthausen, *Chem. Eur. J.* **2008**, *14*, 4318–4327.
[15] E. Rezabal, L. Ducháčková, P. Milko, M. C. Holthausen, J. Roithová, *Inorg. Chem.* **2010**, *49*, 8421–8429.
[16] O. Sander, A. Henß, C. Näther, C. Würtele, M. C. Holthausen, S. Schindler, F. Tuczek, *Chem. Eur. J.* **2008**, *14*, 9714–9729.
[17] M. Schatz, V. Raab, S. P. Foxon, G. Brehm, S. Schneider, M. Reiher, M. C. Holthausen, J. Sundermeyer, S. Schindler, *Angew. Chem.* **2004**, *116*, 4460–4464; *Angew. Chem. Int. Ed.* **2004**, *43*, 4360–4363.
[18] C. Würtele, E. Gaoutchenova, K. Harms, M. C. Holthausen, J. Sundermeyer, S. Schindler, *Angew. Chem.* **2006**, *118*, 3951–3954; *Angew. Chem. Int. Ed.* **2006**, *45*, 3867–3869.
[19] D. Maiti, D.-H. Lee, K. Gaoutchenova, C. Würtele, M. C. Holthausen, A. A. Narducci Sarjeant, J. Sundermeyer, S. Schindler, K. D. Karlin, *Angew. Chem.* **2008**, *120*, 88–91; *Angew. Chem. Int. Ed.* **2008**, *47*, 82–85.
[20] J. S. Woertink, L. Tian, D. Maiti, H. R. Lucas, R. A. Himes, K. D. Karlin, F. Neese, C. Würtele, M. C. Holthausen, E. Bill, J. Sundermeyer, S. Schindler, E. I. Solomon, *Inorg. Chem.* **2010**, *49*, 9450–9459.
[21] K. Ruth, S. Tüllmann, H. Vitze, M. Bolte, H.-W. Lerner, M. C. Holthausen, M. Wagner, *Chem. Eur. J.* **2008**, *14*, 6754–6770.
[22] K. Ruth, R. E. Dinnebier, S. W. Tönnes, E. Alig, I. Sänger, H.-W. Lerner, M. Wagner, *Chem. Commun.* **2005**, 3442–3444.
[23] R. A. Binstead, J. K. Beattie, *Inorg. Chem.* **1986**, *25*, 1481–1484.
[24] Y. Sohrin, H. Kokusen, M. Matsui, *Inorg. Chem.* **1995**, *34*, 3928–3934.
[25] T. Kitano, Y. Sohrin, Y. Hata, H. Kawakami, T. Hori, K. Ueda, *J. Chem. Soc., Dalton Trans.* **2001**, 3564–3571.
[26] D. L. Reger, J. R. Gardinier, W. R. Gemmill, M. D. Smith, A. M. Shahin, G. J. Long, L. Rebbouh, F. Grandjean, *J. Am. Chem. Soc.* **2005**, *127*, 2303–2316.
[27] D. L. Reger, J. R. Gardinier, M. D. Smith, A. M. Shahin, G. J. Long, L. Rebbouh, F. Grandjean, *Inorg. Chem.* **2005**, *44*, 1852–1866.
[28] S.-J. Chiou, Ph. D. Thesis, University of Delaware, Newark, DE, USA, **2004**.
[29] J. P. Jesson, S. Trofimenko, D. R. Eaton, *J. Am. Chem. Soc.* **1967**, *89*, 3158–3164.
[30] R. A. D. Wentworth, T. S. Piper, *Inorg. Chem.* **1965**, *4*, 709–714.
[31] J. C. Dabrowiak, P. H. Merrell, D. H. Busch, *Inorg. Chem.* **1972**, *11*, 1979–1988.
[32] D. F. Evans, *J. Chem. Soc.* **1959**, 2003–2005.
[33] E. M. Schubert, *J. Chem. Educ.* **1992**, *69*, 62.
[34] A. Fouqueau, S. Mer, M. E. Casida, L. M. Lawson Daku, A. Hauser, T. Mineva, F. Neese, *J. Chem. Phys.* **2004**, *120*, 9473–9486.
[35] M. Swart, *J. Chem. Theory Comput.* **2008**, *4*, 2057–2066.
[36] I. Respondek, L. Bressel, P. Saalfrank, H. Kämpf, A. Grohmann, *Chem. Phys.* **2008**, *347*, 514–522.
[37] S. Ye, F. Neese, *Inorg. Chem.* **2010**, *49*, 772–774.
[38] M. Güell, M. Solà, M. Swart, *Polyhedron* **2010**, *29*, 84–93.
[39] H. Paulsen, A. X. Trautwein, *J. Phys. Chem. Solids* **2004**, *65*, 793–798.
[40] S. Zein, S. A. Borshch, P. Fleurat-Lessard, M. E. Casida, H. Chermette, *J. Chem. Phys.* **2007**, *126*, 014105.
[41] R. H. Blessing, *Acta Crystallogr., Sect. A* **1995**, *51*, 33–38.
[42] A. L. Spek, *J. Appl. Crystallogr.* **2003**, *36*, 7–13.
[43] G. M. Sheldrick, *Acta Crystallogr., Sect. A* **1990**, *46*, 467–473.
[44] G. M. Sheldrick, *SHELXL-97. A Program for the Refinement of Crystal Structures*, University of Göttingen, Göttingen, Germany, **1997**.
[45] A. D. Becke, *Phys. Rev. A* **1988**, *38*, 3098–3100.
[46] C. Lee, W. Yang, R. G. Parr, *Phys. Rev. B* **1988**, *37*, 785–789.
[47] P. J. Stephens, F. J. Devlin, C. F. Chabalowski, M. J. Frisch, *J. Phys. Chem.* **1994**, *98*, 11623–11627.
[48] A. D. Becke, *J. Chem. Phys.* **1993**, *98*, 5648–5652.
[49] M. Reiher, O. Salomon, B. A. Hess, *Theor. Chem. Acc.* **2001**, *107*, 48–55.
[50] O. Salomon, M. Reiher, B. A. Hess, *J. Chem. Phys.* **2002**, *117*, 4729–4737.
[51] J. P. Perdew, K. Burke, M. Ernzerhof, *Phys. Rev. Lett.* **1996**, *77*, 3865–3868.
[52] a) N. C. Handy, A. J. Cohen, *Mol. Phys.* **2001**, *99*, 403–412; b) W.-M. Hoe, A. J. Cohen, N. C. Handy, *Chem. Phys. Lett.* **2001**, *341*, 319–328.
[53] M. J. Frisch, G. W. Trucks, H. B. Schlegel, G. E. Scuseria, M. A. Robb, J. R. Cheeseman, G. Scalmani, V. Barone, B. Mennucci, G. A. Petersson, H. Nakatsuji, M. Caricato, X. Li, H. P. Hratchian, A. F. Izmaylov, J. Bloino, G. Zheng, J. L. Sonnenberg, M. Hada, M. Ehara, K. Toyota, R. Fukuda, J. Hasegawa, M. Ishida, T. Nakajima, Y. Honda, O. Kitao, H. Nakai, T. Vreven, J. A. Montgomery Jr., J. E. Peralta, F. Ogliaro, M. Bearpark, J. J. Heyd, E. Brothers, K. N. Kudin, V. N. Staroverov, R. Kobayashi, J. Normand, K. Raghavachari, A. Rendell, J. C. Burant, S. S. Iyengar, J. Tomasi, M. Cossi, N. Rega, J. M. Millam, M. Klene, J. E. Knox, J. B. Cross, V. Bakken, C. Adamo, J. Jaramillo, R. Gomperts, R. E. Stratmann, O. Yazyev, A. J. Austin, R. Cammi, C. Pomelli, J. W. Ochterski, R. L. Martin, K. Morokuma, V. G. Zakrzewski, G. A. Voth, P. Salvador, J. J. Dannenberg, S. Dapprich, A. D. Daniels, O. Farkas, J. B. Foresman, J. V. Ortiz, J. Cioslowski, D. J. Fox, *Gaussian 09*, rev. A.02, Gaussian, Inc., Wallingford CT, **2009**.
[54] S. Grimme, *J. Comput. Chem.* **2006**, *27*, 1787–1799.
[55] A. Schäfer, H. Horn, R. Ahlrichs, *J. Chem. Phys.* **1992**, *97*, 2571–2577.

[56] A. Schäfer, C. Huber, R. Ahlrichs, *J. Chem. Phys.* **1994**, *100*, 5829–5835.
[57] F. Weigend, R. Ahlrichs, *Phys. Chem. Chem. Phys.* **2005**, *7*, 3297–3305.
[58] F. Neese, *ORCA – an ab initio, density functional, and semiempirical program package*, version 2.8, University of Bonn, Bonn, Germany, **2010**.
[59] S. Grimme, J. Antony, S. Ehrlich, H. Krieg, *J. Chem. Phys.* **2010**, *132*, 154104.
[60] F. Neese, G. Olbrich, *Chem. Phys. Lett.* **2002**, *362*, 170–178.
[61] F. Neese, *J. Comput. Chem.* **2003**, *24*, 1740–1747.
[62] F. Neese, F. Wennmohs, A. Hansen, U. Becker, *Chem. Phys.* **2009**, *356*, 98–109.
[63] F. Weigend, *Phys. Chem. Chem. Phys.* **2006**, *8*, 1057–1065.
[64] A. Klamt, G. Schüürmann, *J. Chem. Soc. Perkin Trans. 2* **1993**, 799–805.

Received: May 18, 2010
Revised Version Received: February 10, 2011
Published Online: March 4, 2011

